Catalysis Today xxx (xxxx) xxx

Contents lists available at ScienceDirect

Catalysis Today

journal homepage: www.elsevier.com/locate/cattod

Strong metal-support interaction (SMSI) of Pt/CeO_2 and its effect on propane dehydrogenation

Johnny Zhu Chen [a,1], Abhijit Talpade [a,1], Griffin A. Canning [b], Paige R. Probus [a], Fabio H. Ribeiro [a,*], Abhaya K. Datye [b,*], Jeffrey T. Miller [a,*]

[a] Davidson School of Chemical Engineering, Purdue University, 480 Stadium Mall Drive, IN 47906, United States
[b] Department of Chemical and Biological Engineering and Center for Microengineered Materials, University of New Mexico, Albuquerque, NM 87131, United States

ARTICLE INFO

Keywords:
SMSI effect on propane dehydrogenation
Strong metal-support interaction (SMSI)
Pt/CeO_2 propane dehydrogenation catalyst
Electronic effect of SMSI
Geometric effect of SMSI

ABSTRACT

Upon reduction at 975 °C, a strong metal-support interaction (SMSI) of CeO_2 on Pt NPs leads to low rates for ethylene hydrogenation and propane dehydrogenation, but high olefin selectivity for the latter reaction. By contrast, reduction at 550 °C of Pt/CeO_2, leads to 5 nm Pt NP's with ethylene hydrogenation and propane dehydrogenation TORs and low olefin selectivity similar to Pt/SiO_2. X-ray absorption fine structure (EXAFS) and scanning transmission electron microscopy (STEM) shows formation of ~15 nm monometallic Pt nanoparticles partially covered by SMSI CeO_2. The propylene selectivity of Pt NP's covered by SMSI CeO_2 was ~95 % suggesting there were few Pt ensembles capable of catalysing propane hydrogenolysis; while the remaining exposed Pt remain active for dehydrogenation reactions.

1. Introduction

Investigation of supported metal catalysts mostly focuses on optimizing the composition, or geometry of the metal sites to improve the catalytic performance [1–3]. On the other hand, strong metal-support interaction (SMSI) has been also exploited to modify catalytic rates and selectivity. Tauster et al. found that high temperature reduction of group VIII NPs supported on oxides like TiO_2, Nb_2O_5 and FeO_x caused the CO and H_2 chemisorption to be strongly suppressed; while NPs reduced at low temperature displayed normal chemisorption behaviour [4–7]. It is generally thought that these SMSI oxides are partially reduced at high temperature where the sub-stoichiometric oxides migrate and encapsulate metal NPs blocking the catalytic surface, as demonstrated via HRTEM imaging of Rh/TiO_2 [8]. The SMSI overlayers can also change the surface geometric and electronic properties of the group VIII NPs leading to modified catalytic properties [9]. For example, Matsubu et al. found that the formation of a permeable HCO_x overlayer resulted in catalysts with higher CO selectivity for CO_2 reduction [10]. Worz et al. showed that partially reduced SMSI TiO_2 on Au NPs increases the activity for CO oxidation [11]. It was proposed that Au binds to oxygen vacancy sites in the SMSI support leading to an electron transfer from the support to Au. Kang et al. found that Pd NPs supported on TiO_2 were electron rich, compared to non-SMSI Pd, leading to weaker adsorption of acetylene, resulting in higher selectivity for the selective hydrogenation to ethylene [12]. Liu et al. showed that Pt/FeO_x exhibited higher catalytic activity for low temperature CO oxidation due to formation of dual reaction sites, i.e., Pt sites for CO and FeOx sites for O_2 [6].

CeO_2 is also known to exhibit SMSI, however, generally under more extreme temperatures than, for example, TiO_2 [13,14]. In this study, we prepared Pt/CeO_2 catalysts, which have previously been shown to disperse as single atoms on the surface of the CeO_2 by air oxidation at temperatures higher than about 800 °C [15,16]. Pt/CeO_2 catalysts in this study were reduced at 550 °C and 975 °C and showed SMSI characteristics at the higher reduction temperature. Structural characterization by extended X-ray absorption fine structure (EXAFS), X-ray absorption near edge structure (XANES) and scanning transmission electron microscopy (STEM) confirm the formation of monometallic Pt NPs at both reduction temperatures. After reduction at 550 °C, the TOR for ethylene hydrogenation and propane dehydrogenation was similar to that of Pt/SiO_2, a non-SMSI support. After reduction at 975 °C, however, the rate per mol of Pt for ethylene hydrogenation is significantly lower. STEM shows a CeO_x surface coverage on the Pt NPs, i.e., an SMSI state. After reduction at 975 °C, however, Pt/CeO_2 showed much higher olefin

* Corresponding authors.
E-mail addresses: fabio@purdue.edu (F.H. Ribeiro), dayte@unm.edu (A.K. Datye), mill1194@purdue.edu (J.T. Miller).
[1] Equal contribution.

https://doi.org/10.1016/j.cattod.2020.06.075
Received 18 April 2020; Received in revised form 10 June 2020; Accepted 29 June 2020
Available online 12 August 2020

selectivity for propane dehydrogenation (at 550 °C). The higher olefin selectivity is suggested to result from a decrease in the size of exposed Pt ensemble sites responsible for hydrogenolysis, from the partially covered SMSI Pt/CeO_2; while the remaining exposed sites are active for dehydrogenation.

2. Materials and methods

2.1. Catalyst preparation

The procedure for 1% Pt/CeO_2 synthesis followed previous procedure by Lu *et al.* [17]. 1 wt% Pt on CeO_2 was prepared by incipient wetness impregnation of a tetraammineplatinum (II) platinum nitrate (Sigma-Aldrich, 99.995 %) solution onto a commercial ceria support (Solvay, HS5). The fresh catalysts has a surface area of 90 m^2/g for with a pore volume of ceria (0.6 mL/g) was determined by wetting the dry ceria powder with water. The solution was impregnated 6 times with 3 h of drying at 110 °C between each impregnation. The catalyst was then calcined in flowing air at 800 °C for 10 h to atomically disperse Pt in the CeO_2 support. The surface area was 45 m^2/g after 800 °C in air.

The monometallic Pt catalyst with 2 wt% Pt loading was prepared by a pH adjusted incipient wetness impregnation method (IWI) on SiO_2. Pt$(NH_3)_4(NO_3)_2$ was dissolved in 2 mL deionized water and ammonium hydroxide solution was added to adjust the pH to 11. The solution was added dropwise to Davisil Grade 636 silica (pore size =60 Å, surface area = 480 m^2/g). This catalyst was then dried overnight at 125 °C and calcined at 225 °C for 3 h to keep the particle size small. Finally, all the catalysts were pre-reduced in 5% H_2/N_2 (100 mL/min) at 200 °C for 30 min to initially form reduced NP's. These were further pre-reduced for 30 min at 550 or 975 °C.

2.2. In situ X-ray absorption spectroscopy (XAS)

In situ XAS experiments were completed at the Advanced Photon Source (APS), Argonne National Laboratory at the 10-ID beamline. Experiments were performed in florescence mode at the Pt L_3 (11.564 keV) edge. To perform experiments, the catalysts were crushed into a powder and pressed into a stainless-steel sample holder with the catalyst wafer oriented 45 degrees relative to the x-ray beam. The cell used for fluorescence measurement consists of a water-cooled stage fitted with Kapton windows for fluorescence measurement. For treatments, the cell is equipped with water cooling and ceramic heaters for temperature control and valves for gas flow. 3.5 % H_2/He (Airgas) was used to treat the sample cell at 550 °C for 30 min. He (Airgas) was flowed between each temperature exposure to cool the cell to room temperature. The cell was then sealed and moved to the beamline to perform the *in situ* XAS experiment. To reduce potential O_2 exposure, a He tank was connected to the gas purifier.

Each experiment required a concurrent measurement of a Pt foil scan acquired from a third ion chamber for internal energy calibration. Demeter 0.9.25 was the software package used to fit the XAS data. The XANES spectra was used to determine the edge energy using the maximum of the first peak in the first derivative of the spectra. To obtain EXAFS coordination parameters, least-squares fit in R-space of the k^2 -weighted Fourier transform data from 3.0 $Å^{-1}$ to 12.0 $Å^{-1}$ was utilized. 0.80 was determined to be the amplitude reduction factor (S_0^2) by fitting a reference spectrum of Pt foil and using it to fit all other EXAFS spectra. One Pt-Pt path and three free parameters were used for the initial fitting for Pt/CeO_2.

2.3. Propane dehydrogenation catalytic performance tests

Catalytic performance was tested in a fixed bed reactor with a quartz reactor tube of 3/8-inch OD. The temperature of the reactor was controlled by a furnace connected to a controller. To measure catalyst temperature, a K-type thermocouple (O.D. = 3.2 mm) was positioned in the middle of the catalyst bed. 10 mg–200 mg of catalyst was diluted with enough silica to total 1.0 g and loaded into the reactor. The pre-reduced catalyst was re-reduced at 550 °C or 975 °C with 100 ccm 5% H_2/N_2 for 30 min. Propane dehydrogenation was performed with 2.5 % C_3H_8 and 2.5 % H_2, balanced with N_2 at 550 °C. Since the catalysts deactivate, the selectivity and conversion were obtained with fresh catalyst by measuring the performance after about 2 min on stream and every few minutes for 30−60 min. The selectivity and conversion were extrapolated back to zero time, i.e., zero coke on catalyst. A fresh sample of catalyst was measured at each space velocity, and the reproducibility of selectivity is about 3% and rate about 10 %. A Hewlett Packard 6890 Series gas chromatograph using a flame ionization detector (FID) with a Restek Rt-Alumina Bond/Na_2SO_4 GC column (30 m in length, 0.32 mm ID, and 0.5 μm film thickness was used to analyze the products.

2.4. Ethylene hydrogenation catalytic performance tests

Ethylene hydrogenation experiments were carried out in a U-tube quartz reactor (3/8 inch OD). The reactor was loaded with quartz wool before adding the catalyst, amount based on space velocity. The space velocity was adjusted to ensure conversions < 5 %. The thermocouple well inside the reactor was used to monitor the temperature of the catalyst bed. In a typical experiment, 3 torr ethylene (1 % C_2H_4 in 5 % Argon, balance Helium, Matheson Gas Company), 15 torr hydrogen (5 % H_2, balance N_2, Indiana Oxygen Company) and balance UHP (ultra-high purity) nitrogen (Indiana Oxygen Company). The effluent stream was analysed with a Gas Chromatography unit equipped with a Flame Ionization Detector using a GS-Alumina (Agilent J&W) capillary column.

2.5. Scanning transmission Electron microscopy (STEM)

Catalyst was mounted on holey carbon grids for imaging with an FEI Titan transmission electron microscope operated at 300 kV with image aberration correction for TEM images, or a JEOL NEOARM microscope operated at 300 kV with probe aberration correction for STEM images. Samples were mounted on the grids by a dry loading technique in order to eliminate the possibility of carbon contamination to ensure a fair comparison between as prepared, reduced catalyst.

3. Results

3.1. STEM/TEM

Fig. 1 shows a high magnification image of a 1 wt.% Pt-CeO_2 sample that has been calcined at 800 °C, and subsequently reduced at 975 °C or 550 °C in H_2, Fig. 1A, B and C, respectively. Similar to previous reports [15,16,18,19] calcination of Pt on CeO_2 at temperatures above 800 °C leads to isolated Pt atoms, which are shown as bright spots marked by the arrows. After reduction at 975 °C, the Pt NPs are approximately 15 nm. These also show a thin coating of CeO_x on the NP surface, i.e., the faint region highlighted by the white arrow in 1B. This thin film is present across the entire surface of the ceria and is visible as a disruption to the ceria lattice planes at the edges of ceria particles. Previously, HR-TEM has shown that after high temperature reduction Pt_3Ce [20] and $CePt_5$ [21] intermetallic alloys are formed. For this catalyst, all particles index to metallic Pt, see the Fourier Transform the Pt NP (inset in Fig. 1B).

The 1 wt.% Pt-CeO_2 sample was also reduced at 550 °C, Fig. 1C and the average size of the Pt NPs is about 5 nm, which is slightly larger than the benchmark 2−3 nm 2 Pt/SiO_2 catalyst (Fig. S1). In agreement with previous results by Bernal et al. [21], unlike the case of titania [22], 550 °C reduction does not exhibit well defined amorphous coatings, as shown in Fig. 1B. These Pt particles are too small for direct detection of surface features due to the very low contrast in bright field TEM.

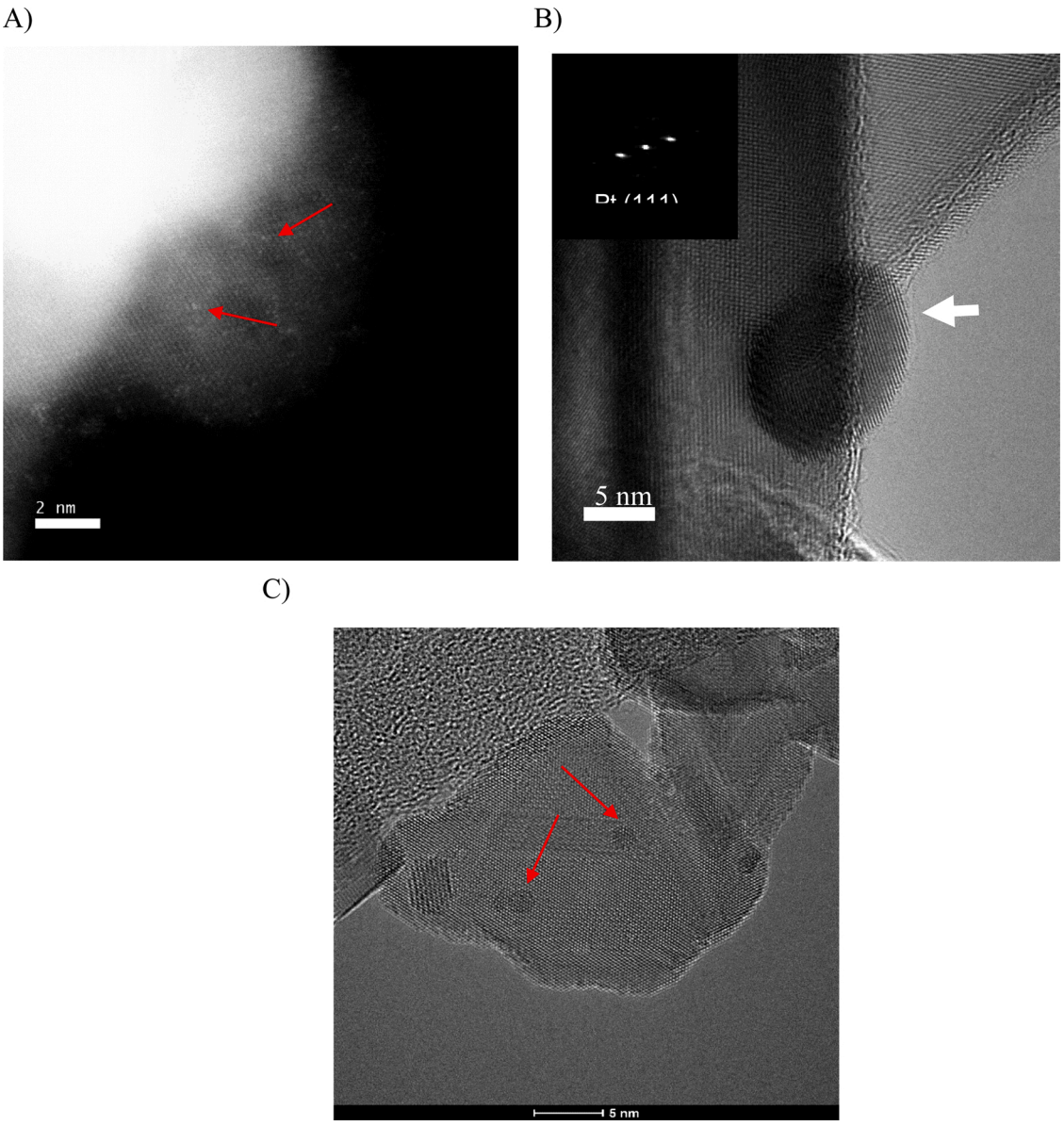

Fig. 1. 1 wt% Pt on ceria, A. Calcined at 800 °C showing single Pt atoms on the CeO_2 support, B. reduced at 975 °C, with faint over layer of CeO_x covering the surface of the NP (white arrow), and C. reduced Pt NP's at 550 °C without a CeO_x overlayer.

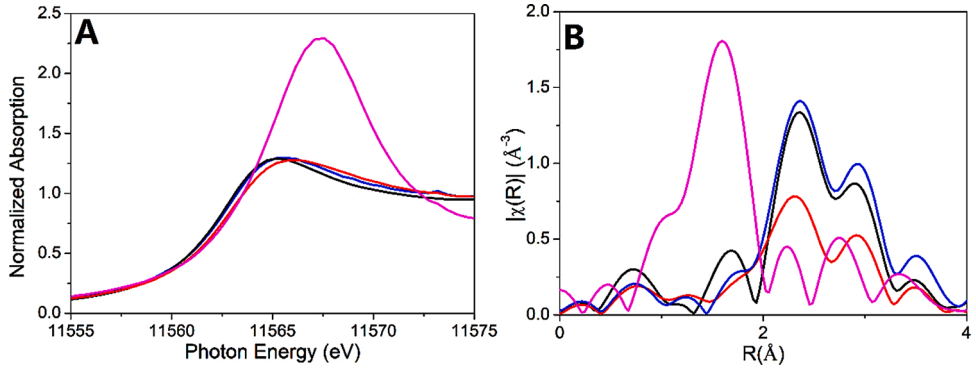

Fig. 2. (A) Pt L_{III} edge XANES spectra of Pt foil (blue), 1 Pt/CeO_2 calcined at 800 °C (magenta), 1 Pt/CeO_2 reduced at 975 °C (black) and 1 Pt/CeO_2 reduced at 550 °C (red). (B) Pt L_{III} edge EXAFS spectra of Pt foil (blue), 1 Pt/CeO_2 reduced at 975 °C (black), 1 Pt/CeO_2 calcined at 800 °C (magenta) and 1 Pt/CeO_2 reduced at 550 °C (red).

3.2. In situ X-ray absorption spectroscopy (XAS)

The Pt L_3 edge X-ray absorption near edge structure (XANES) and extended X-ray absorption fine structure (EXAFS) spectra for the single atom 1 Pt/CeO_2 oxidized at 800°C has previously been reported [18,19]. Similar results have been found in this study shown in Fig. 2 and Table 1. These have a XANES energy and high white line intensity typical of Pt^{2+} ions with a first shell Pt-O coordination of 5 at 2.05 Å, with a small second shell scattering peak characteristic of isolated atoms. The Pt L_3 XANES for Pt/CeO_2 reduced at 550°C and 975 °C are shown in Fig. 2(B). After 550 °C and 975 °C reduction, 1 Pt/CeO_2 had an edge energy of 11564.0 eV, which is identical to Pt foil and consistent with monometallic 2−3 nm Pt/SiO_2 nanoparticles (Fig. S2(A)).

For 1 Pt/CeO_2 reduced at 550 °C and 975 °C, the Pt L_3 magnitude of the Fourier transform of the k^2-weighted EXAFS shows three main peaks between 2−3 Å in Fig. 2(B), which is typical of the Pt-Pt scattering in metallic Pt NPs (Fig. S2(B)). The magnitude of the peaks was smaller when 1 Pt/CeO_2 was reduced at 550 °C indicating a smaller particle size. The fit of the EXAFS for Pt/CeO_2 reduced at 975 °C, gave a Pt-Pt had a coordination of 10.8 and bond distance similar to that of Pt foil (Table 1), consistent with the TEM particle size (>10 nm). The fit of the EXAFS for Pt/CeO_2 reduced at 550 °C gave a Pt-Pt coordination number of 8.5 with bond distance of 2.74 Å, slightly shorter than Pt foil, and consistent with about 5 nm NPs consistent with TEM. The EXAFS fit of Pt/SiO_2 was 7.6 at 2.73 Å, consistent with slightly smaller NPs on Pt/CeO_2 reduced at 550 °C.

3.3. Ethylene hydrogenation

Hydrogenation of ethylene is a structure sensitive reaction where every exposed Pt has the same TOR independent of the particle size or support type, thus can be used to determine the number of active surface Pt sites [23–25]. In this study, this reaction will be used to estimate the number of (metallic) catalytic Pt sites for the Pt/CeO_2 catalysts under different treatment conditions, i.e., air at 800 °C, and 550, 900 or 975 °C reduction with H_2.

As shown in Table 2, the fresh (air at 800°C) Pt/CeO_2 catalysts shows low rates per g Pt for ethylene hydrogenation. Since the STEM shows that these are atomically dispersed, the turnover rate (TOR) was determined assuming each Pt is active. The TOR of 7×10^{-4} s^{-1} is much smaller than that reported for metallic Pt [24,26,27].

Following reduction in H_2 at 550 °C, the rate/g Pt increased to 4.3×10^{-1} s^{-1}, almost 3 orders of magnitude higher than atomically dispersed Pt^{2+} ions. Estimating the dispersion from the TEM particle size of 5 nm, i.e., 20 % dispersion, the TOR is 1.1 s^{-1}. The TOR of a 2 wt.% Pt/SiO_2 reduced at 550 °C with a dispersion of 0.44, determined by CO chemisorption, was 1.4 s^{-1} and similar to rates reported for other Pt catalysts [23,24,26,28]. Thus, Pt/CeO_2 reduced at 550 °C has a TOR typical of other non-SMSI Pt catalysts.

Table 1
XAS parameters for different catalysts.

Catalyst and treatment	XANES edge energy (eV)	Scattering Pair	Coordination Number	Bond distance (Å)	σ^2 (Å^2)
1Pt/CeO_2, 800 °C air	11565.6	Pt-O	5.2±0.5	1.98±0.03	0.002
1Pt/CeO_2, 550 °C/H_2	11564.0	Pt-Pt	8.5±0.4	2.74±0.01	0.007
1Pt/CeO_2, 975 °C/H_2	11564.0	Pt-Pt	10.8±0.3	2.76±0.02	0.006
2Pt/SiO_2, 975 °C/H_2	11564.0	Pt-Pt	7.6±0.4	2.73±0.01	0.005
Pt foil	11564.0	Pt-Pt	12.0±0.4	2.76±0.01	0.003

Table 2
Ethylene hydrogenation tests on 1% Pt/CeO2 using different pre-treatments.

Catalyst Pretreatment	Rate[a] (μmol/g/s)	TOR[b] (10^{-1} s^{-1})
Air/800°C	0.04	0.0007
*H_2/550°C	22.0	1.1
H_2/900 °C	0.5	–
H_2/975 °C	0.4	–

Reduction with 5% H_2 for 30 min at the defined temperatures.
Reaction conditions: P (C_2H_4) = 3 torr, P(H_2) = 15 torr, T=30 °C. Catalyst diluted to a ratio of 1:16 using Davisil grade SiO_2. Space velocity = 20 L hr^{-1} $gcat^{-1}$. Conversions for all the experiments < 5 %.
[*] Space velocity = 100 L hr^{-1} $gcat^{-1}$, Dilution ratio 1:100 (to maintain < 5 % conversion).
[a] Initial ethane formation rate based on the Pt loading.
[b] Initial TOF calculated based TEM particle size, 5 nm.

At higher reduction temperatures (900 °C and 975 °C), however, the ethylene hydrogenation rate/g Pt decreases significantly. At 975 °C, for example, the Pt NPs are larger, ca. 15 nm, or an estimated dispersion of about 6–7 %. If the loss in rate were due to sintering alone, the rate/g would be about 3 times lower, e.g., 20/6.5, or the ratio of dispersions, than Pt/CeO_2 reduced at 550°C. The rates per/g, however, are 40–50 times lower, which far exceeds that from sintering alone. The large decrease in rate is likely due to the blockage of surface Pt sites by the CeO_x over layers as evidenced in Fig. 1B. The very low ethylene hydrogenation rates suggest that only a small fraction of the Pt surface is catalytic.

Previously, CeO_2 has been shown to exhibit an SMSI effect at relatively moderate temperatures (>300 °C) and inhibit the activity of noble metal catalysts [29–31]. Cunningham et al. studied the effect of H_2 pretreatment on a Rh/CeO_2 catalyst at temperatures up to 380 °C and found complete loss of activity for acetone hydrogenation [32]. Liotta et al. observed similar results with reduced activity for NO reduction by C_3H_6 for Pt/ceria-zirconia catalysts reduced in H_2 at elevated temperature. Small angle X-ray scattering (SAXS) and XPS were used to detect the SMSI state [33]. Other studies show high reduction temperatures are required for SMSI on Pt/CeO_2. Reduction of Pt/CeO_2 at 700 °C was highly selectivity for crotonaldehyde hydrogenation. The improved performance was due to preferential hydrogenation of the carbonyl group for Pt NPs existing in an SMSI state [34]. In our catalysts, we observe little effect of SMSI at 550 °C, but the Pt NPs have high surface CeO_2 coverage after reduction above 900 °C, much higher than generally reported.

3.4. Propane dehydrogenation

These Pt/CeO_2 catalysts, and for comparison Pt/SiO_2, were also evaluated for propane dehydrogenation. Hydrogen was co-fed in order to increase the hydrogenolysis selectivity forming methane, ethane and ethylene, which is a more severe evaluation of the catalyst's performance. Each data point was determined with fresh catalyst at different space velocity, i.e., sample weight or flow. To obtain the coke-free activity and selectivity, the conversion and selectivity was determined after about 2 min and every few minutes for about 30−60 min and extrapolated to zero time. As shown in Fig. 3 (pink), the propylene selectivity of 2 Pt/SiO_2 was 75 % at 15 % conversion, and the selectivity decreases as the conversion increases, for example about 60 % at 30 % conversion. The TOR was 0.17 s^{-1} (Table 3), which is consistent with previous literature [35]. For 1 Pt/CeO_2 reduced at 550 °C (Fig. 3 (black)), the selectivity was slightly higher, but similar to 2 Pt/SiO_2 and the TOR was also similar. Thus, the catalytic performance of 1 Pt/CeO_2 reduced at 550 °C is very similar to 2 Pt/SiO_2. For 1 Pt/CeO_2 reduced at 975 °C (Fig. 3 (blue)), however, the propylene selectivity was much higher, about 94 %, than for reduction at 550 °C. In addition, the olefin

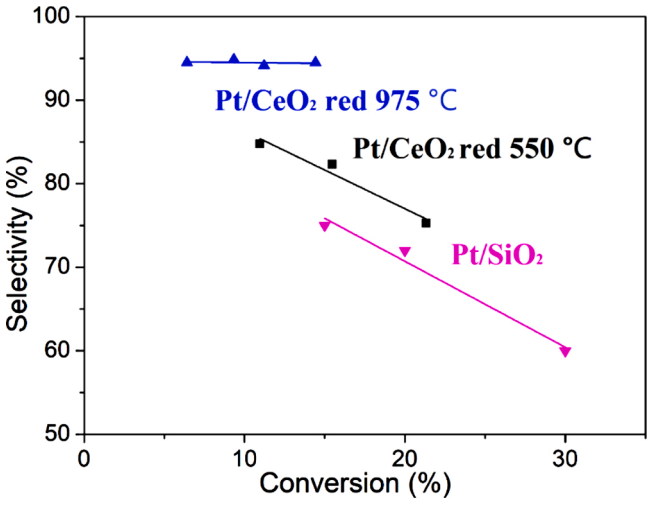

Fig. 3. Propylene selectivity at different conversions of 1 Pt/CeO2 reduced at 975 °C (blue, upwards triangle), 1 Pt/CeO_2 reduced at 500 °C (black square), and 2 Pt/SiO_2 (pink inverted triangle). Reaction conditions: 550 °C, 2.5 % C_3H_8 + 2.5 % H_2 balanced with N_2.

Table 3
Summary of catalytic results for propane dehydrogenation.

Sample Name	Rate (mol/(s*mol catalyst))	Initial Turnover Rate (s^{-1})
2 Pt/SiO_2	0.077	0.17
Pt/CeO_2-red550°C	0.065	0.33
Pt/CeO_2-red975°C	0.00085	0.013

Reaction conditions: 550 °C, 2.5 % C_3H_8 + 2.5 % H_2 balanced with N_2; selectivity and TOR calculated at 10 % C_3H_8 conversion; Pt/SiO_2 TOR based on CO chemisorption (44 %) and Pt/CeO_2 calculated from TEM particle size; 550 °C (5 nm-20 % dispersion) and 975 °C (15 nm-6.5 % dispersion).

selectivity remained high with increasing conversion. The rate per g Pt (Table 3), however, was about two orders of magnitude lower than that of the catalyst reduced at 550 °C. The loss in activity is similar to that observed for ethylene hydrogenation. The TOR based on the STEM size also indicates a much lower rate, about 25 times lower than non-SMSI catalysts. However, the TOR based on the number is sites estimated from the ethylene hydrogenation rate is similar to non-SMSI Pt NPs.

4. Discussion

4.1. Structure of Pt/CeO_2 catalysts

Similar to previous studies, Pt single atoms are dispersed on the CeO_2 after 800 °C calcination [15,16,18,19]. These, however, have low catalytic activity compared to Pt NPs and are readily reduced to Pt NP's at temperatures above about 300 °C. The *in situ* XAS and STEM structure determination of Pt/CeO_2, reduced at 975 °C, indicate that monometallic Pt NPs are present with no evidence for formation of any intermetallic alloy, as previously reported [35–40]. At 550 °C, the Pt NPs are approximately 5 nm, with no evidence of a CeO_x SMSI oxide layer. The catalytic TOR of ethylene hydrogenation is similar to Pt/SiO_2 and the propane dehydrogenation TOR and selectivity are also similar, consistent with no change in the catalytic properties due to a support interaction. Reduction after 975 °C, however, led to the formation of an oxide over layer observed by STEM, Fig. 1B, and a significant loss in the TOR for ethylene hydrogenation consistent with a CeO_x SMSI structure. The formation of the SMSI oxide, however, occurred at much higher temperature than reported for Pt/TiO_2, for example, which occurs at about 500 °C [4,5]. This high reduction temperature to form a CeO_2 SMSI state is consistent with a previous study by Deleitenburg et al. showing that CeO_2 only exhibits SMSI behavior under extremely harsh conditions. At these high temperatures, the Pt NPs also sinter (ca. 15 nm) compared to the particles reduced at lower temperature (5 nm).

SMSI oxides are often suggested to increase number of electrons on the metal NPs by transfer of electron density from the partially reduced support. For example, it has been shown by XPS that the $4f_{7/2}$ peak is shifted from 71.0 eV (Pt) to 70.2 eV (Pt/TiO_2) suggesting that TiO_2 provided electrons to the Pt nanoparticles [41,42]. In this study, the XANES edge energy of Pt/CeO_2 after reduction at 550 and 975 °C are very similar suggesting little change in the Pt.

4.2. The effect of SMSI on catalyst performance

The TOR of Pt NPs is independent of particle size and support for ethylene hydrogenation; thus, one can estimate the SMSI coverage of the Pt NPs from the apparent TOR for the Pt/CeO_2 reduced at 975 °C. From the STEM images, the particle size of the latter is about 15 nm, which corresponds to ~6% of dispersion [43]. However, the apparent TOR is much lower. Assuming that the loss in rate is due to surface coverage by SMSI CeO_2, approximately 90 % of the catalytic sites are inaccessible for catalysis. Of the few remaining exposed sites, there is a significant increase in the olefin selectivity for propane dehydrogenation.

Alkane dehydrogenation, which is the reverse reaction of olefin hydrogenation is a structure insensitive reaction, thus, only requires individual atoms for catalytic activity. Hydrogenolysis, a structure sensitive reaction, requires several atom ensemble active sites [44]. Intermetallic alloys such as Pt_3Mn, [45] Pt_3Co, [40] Pt_1Bi_1 [39], Pt_3Cr, [37] Pt_3V [46] and Pt_1Zn_1 [36] have been shown to have isolated or three atom ensemble Pt sites and are highly olefin selective for alkane dehydrogenation. While *in situ* EXAFS and STEM suggested that Pt/CeO_2 did not form an alloy even after 975 °C reduction, the high propylene selectivity suggests that the ensemble size of the catalyst was likely significantly reduced. Previous studies have shown that SMSI catalysts inhibits hydrogenolysis. Ethane hydrogenolysis has been suppressed on Pd/TiO_2 in a study by Bracery et al.; while HDO of m-Cresol on NiMo/SiO_2 catalyst also showed hydrogenolysis suppression [47,48]. Therefore, the higher propylene selectivity is likely that due to the high surface coverage of these large Pt NPs by CeO_x resulting in few ensemble sites capable of hydrogenolysis.

5. Conclusion

In summary, single atom Pt sites on CeO_2 have low catalytic rates for hydrogenation and are readily reduced to Pt NPs at temperatures above about 300 °C. Small to moderate sized NPs formed at temperatures below about 550 °C, display normal Pt catalytic properties for ethylene hydrogenation and propane dehydrogenation with no evidence of an SMSI CeO_x by catalysis or STEM. Reduction at 975 °C leads to sintering of the Pt NPs to about 15 nm and coverage of greater than about 90 % of these larger particles by an SMSI CeO_x. Both sintering and SMSI lead to a large loss in catalytic rate. The small number of exposed Pt sites on SMSI Pt/CeO_2, however, led to highly selective propane dehydrogenation catalysts compared to Pt/SiO_2, for example. The high olefin selectivity is likely due to smaller Pt ensembles, which suppress hydrogenolysis reactions, while the few remaining exposed Pt sites are active for dehydrogenation.

Declaration of Competing Interest

The authors report no declarations of interest.

Acknowledgements

This work was supported by the National Science Foundation under Cooperative Agreement No. EEC-1647722. Use of the Advanced Photon Source was supported by the U.S. Department of Energy Office of Basic

Energy Sciences under contract no. DE-AC02-06CH11357. MRCAT operations, beamline 10-ID, are supported by the Department of Energy and the MRCAT member institutions. This work was performed, in part, at the Center for Integrated Nanotechnologies, an Office of Science User Facility operated for the U.S. Department of Energy (DOE) Office of Science by Los Alamos National Laboratory (Contract 89233218CNA000001) and Sandia National Laboratories (Contract DE-NA-0003525). This work was performed, in part, with the help of John D Watt at the Center for Integrated Nanotechnologies, an Office of Science User Facility operated for the U.S. Department of Energy (DOE) Office of Science by Los Alamos National Laboratory (Contract 89233218CNA000001) and Sandia National Laboratories (Contract DE-NA-0003525).

Appendix A. Supplementary data

Supplementary material related to this article can be found, in the online version, at doi:https://doi.org/10.1016/j.cattod.2020.06.075.

References

[1] P. Christopher, S. Linic, Engineering selectivity in heterogeneous catalysis: Ag nanowires as selective ethylene epoxidation catalysts, J. Am. Chem. Soc. 130 (2008) 11264–11265.
[2] F. Calle-Vallejo, J. Tymoczko, V. Colic, Q.H. Vu, M.D. Pohl, K. Morgenstern, D. Loffreda, P. Sautet, W. Schuhmann, A.S. Bandarenka, Finding optimal surface sites on heterogeneous catalysts by counting nearest neighbors, Science 350 (2015) 185–189.
[3] A. Holewinski, J.-C. Idrobo, S. Linic, High-performance Ag–Co alloy catalysts for electrochemical oxygen reduction, Nat. Chem. 6 (2014) 828.
[4] S.J. Tauster, S.C. Fung, R.L. Garten, Strong metal-support interactions - group-8 noble-metal supported on TiO2, J. Am.Chem. Soc. 100 (1978) 170–175.
[5] S.J. Tauster, S.C. Fung, R.T.K. Baker, J.A. Horsley, Strong-interactions in supported-metaal catalysis, Science 211 (1981) 1121–1125.
[6] L.Q. Liu, F. Zhou, L.G. Wang, X.J. Qi, F. Shi, Y.Q. Deng, Low-temperature CO oxidation over supported Pt, Pd catalysts: particular role of FeOx support for oxygen supply during reactions, J. Catal. 274 (2010) 1–10.
[7] G.L. Haller, D.E. Resasco, Metal support interaction - group-VIII metals and reducible oxides, J. Adv. Catal. 36 (1989) 173–235.
[8] A.D. Logan, E.J. Braunschweig, A.K. Datye, D.J. Smith, Direct observation of the surfaces of small metal crystallites: rhodium supported on titania, Langmuir 4 (1988) 827–830.
[9] H.J. Freund, Model studies in heterogeneous catalysis, Chem. Eur. J. 16 (2010) 9384–9397.
[10] J.C. Matsubu, S.Y. Zhang, L. DeRita, N.S. Marinkovic, J.G.G. Chen, G.W. Graham, X.Q. Pan, P. Christopher, Adsorbate-mediated strong metal-support interactions in oxide-supported Rh catalysts, Nat. Chem. 9 (2017) 120–127.
[11] A.S. Wörz, U. Heiz, F. Cinquini, G. Pacchioni, Charging of Au atoms on TiO2 thin films from CO vibrational spectroscopy and DFT calculations, J. Phys. Chem. B 109 (2005) 18418–18426.
[12] J.H. Kang, E.W. Shin, W.J. Kim, J.D. Park, S.H. Moon, Selective hydrogenation of acetylene on TiO2-added Pd catalysts, J. Catal. 208 (2002) 310–320.
[13] C. Deleitenburg, A. Trovarelli, Metal-support interactions in Rh/CeO2, Rh/TiO2, and Rh/Nb2O5 catalysts as inferred from CO2 methanation activity, J. Catal. 156 (1995) 171–174.
[14] A. Caballero, J.P. Holgado, V.M. Gonzalez-delaCruz, S.E. Habas, T. Herranz, M. Salmeron, In situ spectroscopic detection of SMSI effect in a Ni/CeO2 system: hydrogen-induced burial and dig out of metallic nickel, Chem. Comm. 46 (2010) 1097–1099.
[15] J. Jones, H. Xiong, A.T. DeLaRiva, E.J. Peterson, H. Pham, S.R. Challa, G. Qi, S. Oh, M.H. Wiebenga, X.I.P. Hernández, Thermally stable single-atom platinum-on-ceria catalysts via atom trapping, Science 353 (2016) 150–154.
[16] H. Xiong, S. Lin, J. Goetze, P.D. Pletcher, L. Kovarik, K. Artyushkova, H. Guo, B. Weckhuysen, A. Datye, Thermally stable and regenerable Pt-Sn clusters for propane dehydrogenation prepared via atom trapping on Ceria, Angew. Chem. Int. Ed. 56 (2017) 8986–8991.
[17] Y. Lu, C. Thompson, D. Kunwar, A. Datye, A.M.J.C. Karim, Origin of the high CO oxidation activity on CeO2 supported Pt nanoparticles: weaker binding of CO or facile oxygen transfer from the support? ChemCatChem 12 (2020) 1726–1733.
[18] P. Xie, T. Pu, A. Nie, S. Hwang, S.C. Purdy, W. Yu, D. Su, J.T. Miller, C. Wang, Nanoceria-supported single-atom platinum catalysts for direct methane conversion, ACS Catal. 8 (2018) 4044–4048.
[19] D. Kunwar, S. Zhou, A. DeLaRiva, E.J. Peterson, H. Xiong, X.I. Pereira-Hernández, S.C. Purdy, R. ter Veen, H.H. Brongersma, J.T. Miller, Stabilizing high metal loadings of thermally stable platinum single atoms on an industrial catalyst support, ACS Catal. 9 (2019) 3978–3990.
[20] S. Penner, G. Rupprechter, H. Sauer, D.S. Su, R. Tessadri, R. Podloucky, R. Schlögl, K. Hayek, Pt/ceria thin film model catalysts after high-temperature reduction: a (HR) TEM study, Vacuum 71 (2003) 71–76.
[21] S. Bernal, J. Calvino, M. Cauqui, J. Gatica, C. Larese, J.P. Omil, J. Pintado, Some recent results on metal/support interaction effects in NM/CeO2 (NM: noble metal) catalysts, Catal. Today 50 (1999) 175–206.
[22] S. Bernal, J. Calvino, M. Cauqui, G. Cifredo, A. Jobacho, J. Rodriguez-Izquierdo, Metal-support interaction phenomena in rhodium/ceria and rhodium/titania catalysts: comparative study by high-resolution transmission electron spectroscopy, Appl. Catal. A Gen. 99 (1993) 1–8.
[23] F.H. Ribeiro, A.E. Schach Von Wittenau, C.H. Bartholomew, G.A. Somorjai, Reproducibility of turnover rates in heterogeneous metal catalysis: compilation of data and guidelines for data analysis, Catal. Rev. 39 (1997) 49–76.
[24] R.D. Cortright, S.A. Goddard, J.E. Rekoske, J. Dumesic, Kinetic study of ethylene hydrogenation, J. Catal. 127 (1991) 342–353.
[25] F. Zaera, G. Somorjai, Hydrogenation of ethylene over platinum (111) single-crystal surfaces, J. Am. Chem. Soc. 106 (1984) 2288–2293.
[26] J. Schlatter, M. Boudart, Hydrogenation of ethylene on supported platinum, J. Catal. 24 (1972) 482–492.
[27] T.A. Dorling, M.J. Eastlake, R.L. Moss, The structure and activity of supported metal catalysts: IV. Ethylene hydrogenation on platinum/silica catalysts, J. Catal. 14 (1969) 23–33.
[28] J. Grunes, J. Zhu, E.A. Anderson, G.A. Somorjai, Ethylene hydrogenation over platinum nanoparticle array model catalysts fabricated by electron beam lithography: determination of active metal surface area, J. Phys. Chem. B 106 (2002) 11463–11468.
[29] S. Bernal, F. Botana, J. Calvino, M. Cauqui, G. Cifredo, A. Jobacho, J. Pintado, J. Rodriguez-Izquierdo, Microstructural and chemical properties of ceria-supported rhodium catalysts reduced at 773 K, J. Phys. Chem. 97 (1993) 4118–4123.
[30] J.M. Cíes, E. del Río, M. López-Haro, J.J. Delgado, G. Blanco, S. Collins, J. J. Calvino, S. Bernal, Fully reversible metal deactivation effects in gold/ceria–zirconia catalysts: role of the redox state of the support, Angew. Chem. Int. Ed. 49 (2010) 9744–9748.
[31] D. Kalakkad, A.K. Datye, H. Robota, Interaction of platinum and ceria probed by transmission electron microscopy and catalytic reactivity, Appl. Catal. B 1 (1992) 191–219.
[32] J. Cunningham, S. Obrien, J. Sanz, J.M. Rojo, J.A. Soria, J.L.G. Fierro, Exceptional susceptibility of ceria-supported rhodium catalyst to inhibitory SMSI effects including acetone hydrogenation, J. Mol. Catal. 57 (1990) 379–396.
[33] L.F. Liotta, A. Longo, A. Macaluso, A. Martorana, G. Pantaleo, A.M. Venezia, G. Deganello, Influence of the SMSI effect on the catalytic activity of a Pt(1%)/Ce0.6Zr0.4O2 catalyst: SAXS, XRD, XPS and TPR investigations, Appl. Catal. B 48 (2004) 133–149.
[34] A.K. Aboul-Gheit, A.E. Awadallah, A.A. Aboul-Enein, A.-L.H. Mahmoud, Molybdenum substitution by copper or zinc in H-ZSM-5 zeolite for catalyzing the direct conversion of natural gas to petrochemicals under non-oxidative conditions, Fuel 90 (2011) 3040–3046.
[35] Z. Wu, E.C. Wegener, H.-T. Tseng, J.R. Gallagher, J.W. Harris, R.E. Diaz, Y. Ren, F. H. Ribeiro, J.T. Miller, Pd–In intermetallic alloy nanoparticles: highly selective ethane dehydrogenation catalysts, Catal. Sci. Technol. 6 (2016) 6965–6976.
[36] V.J. Cybulskis, B.C. Bukowski, H.-T. Tseng, J.R. Gallagher, Z. Wu, E. Wegener, A. J. Kropf, B. Ravel, F.H. Ribeiro, J. Greeley, Zinc promotion of platinum for catalytic light alkane dehydrogenation: insights into geometric and electronic effects, ACS Catal. 7 (2017) 4173–4181.
[37] N.J. LiBretto, C. Yang, Y. Ren, G.H. Zhang, J.T. Miller, Identification of surface structures in Pt3Cr intermetallic nanocatalysts, Chem. Mater. 31 (2019) 1597–1609.
[38] E.C. Wegener, Z. Wu, H.-T. Tseng, J.R. Gallagher, Y. Ren, R.E. Diaz, F.H. Ribeiro, J. T. Miller, Structure and reactivity of Pt–in intermetallic alloy nanoparticles: highly selective catalysts for ethane dehydrogenation, Catal. Today 299 (2018) 146–153.
[39] J.Z. Chen, Z.W. Wu, X.B. Zhang, S. Choi, Y. Xiao, A. Varma, W. Liu, G.H. Zhang, J. T. Miller, Identification of the structure of the Bi promoted Pt non-oxidative coupling of methane catalyst: a nanoscale Pt3Bi intermetallic alloy, Catal. Sci. Technol. 9 (2019) 1349–1356.
[40] L.G. Cesar, C. Yang, Z. Lu, Y. Ren, G.H. Zhang, J.T. Miller, Identification of a Pt3Co surface intermetallic alloy in Pt-Co propane dehydrogenation catalysts, ACS Catal. 9 (2019) 5231–5244.
[41] J. Ohyama, A. Yamamoto, K. Teramura, T. Shishido, T. Tanaka, Modification of metal nanoparticles with TiO2 and metal-support interaction in photodeposition, ACS Catal. 1 (2011) 187–192.
[42] M.K. Bahl, S.C. Tsai, Y.W. Chung, Auger and photoemission investigations of the platinum-SrTiO3(100) interface: relaxation and chemical-shift effects, Phys. Rev. B 21 (1980) 1344–1348.
[43] A. Borodziński, M. Bonarowska, Relation between crystallite size and dispersion on supported metal catalysts, Langmuir 13 (1997) 5613–5620.
[44] M. Boudart, Heterogeneous catalysis by metals, J. Mol. Catal. 30 (1985) 27–38.
[45] Z.W. Wu, B.C. Bukowski, Z. Li, C. Milligan, L. Zhou, T. Ma, Y. Wu, Y. Ren, F. H. Ribeiro, W.N. Delgass, J. Greeley, G.H. Zhang, J.T. Miller, Changes in catalytic and adsorptive properties of 2 nm Pt3Mn nanoparticles by subsurface atoms, J. Am. Chem. Soc. 140 (2018) 14870–14877.
[46] S. Purdy, P. Ghanekar, G.M. Mitchell, A.J. Kropf, D.Y. Zemlyanov, Y. Ren, F. H. Ribeiro, W.N. Delgass, J.P. Greeley, J.T. Miller, The origin of electronic

modification of platinum in a Pt3V alloy and their consequences for propane dehydrogenation catalysis, ACS Appl. Energy Mater. (2020).

[47] J.D. Bracey, R. Burch, Enhanced activity of Pd/TiO2 catalysts for the CO/H2 reaction in the absence of strong metal-support interactions (SMSI), J. Catal. 86 (1984) 384–391.

[48] F.F. Yang, N.J. Libretto, M.R. Komarneni, W. Zhou, J.T. Miller, X.L. Zhu, D. E. Resasco, Enhancement of m-cresol hydrodeoxygenation selectivity on Ni catalysts by surface decoration of MoOx species, ACS Catal. 9 (2019) 7791–7800.